Levi et al, 2018, Characterizing seismites with anisotropy of magnetic susceptibility: Geology, https://doi.org/10.1130/G45120.1.

Table DR1: AMS data

| Site | Structure type | Rock type | N | $K_m$ | $L^a$ | $P^a$ | $T^a$ | $F^a$ | **Coordinates Lat./Lon.** |
|---|---|---|---|---|---|---|---|---|---|
| PZA | Reference layer | Aragonite | 20 | 48 (11.5) | 1.001* (m.) (0.001) | 1.023* (m.) (0.003) | 0.94* (m.) (0.06) | 1.024* (m.) (0.002) | 31.0993/35.3616 |
| QSOU | Reference layer | Detritus | 10 | 76 (14) | 1.001* (m.) (0.001) | 1.014* (m.) (0.007) | 0.82* (m.) (0.36) | 1.012* (m.) (0.007) | 31.0905/35.3648 |
| MS10 (Masada) | Fold | Aragonite | 17 | 24 (10) | 1.009 (0.007) | 1.033 (0.007) | 0.45 (0.4) | 1.024 () | 31.3059/35.3782 |
| ZIN1 (hangingwall | Fold | Aragonite | 10 | 20 (5.9) | 1.022 (0.005) | 1.039 (0.009) | -0.16 (0.29) | 1.017 (0.008) | 30.9611/35.3021 |
| ZIN1 (Footwall) | Fold | Aragonite | 19 | 16 (7.6) | 1.02 (0.006) | 1.046 (0.01) | 0.11 (0.2) | 1.026 (0.007) | 30.9611/35.3021 |
| ZIN1 (hinge) | Fold | Aragonite | 7 | 29 (10) | 1.019 (0.003) | 1.04 (0.01) | 0.03 (0.2) | 1.021 (0.009) | 30.9611/35.3021 |
| ZIN2 | Fold upper anticline (horizontal layer) | Aragonite | 6 | 33 (3) | 1.008 (0.006) | 1.036 (0.005) | 0.56 (0.27) | 1.028 (0.003) | 30.9611/35.3021 |
| ZIN2 | Fold Hinge | Aragonite | 6 | 29 (10) | 1.01 (0.003) | 1.029 (0.005) | 0.3 (0.24) | 1.019 (0.005) | 30.9611/35.3021 |
| ZIN2 | Fold upper anticline (horizontal layer) | Detritus | 8 | 57 (6) | 1.004 (0.003) | 1.031 (0.002) | 0.71 (0.16) | 1.027 (0.003) | 30.9611/35.3021 |
| ZIN2 | Fold hinge | Detritus | 7 | 46 (16) | 1.014 (0.008) | 1.028 (0.002) | -0.027 (0.5) | 1.013 (0.007) | 30.9611/35.3021 |
| ZIN2.1 | Fold hinge | Aragonite | 8 | 24 (11) | 1.014 (0.002) | 1.034 (0.005) | 0.18 (0.09) | 1.02 (0.003) | 30.9611/35.3021 |
| PZ3 | Fold | Aragonite | 12 | 26 (8.9) | 1.018 (0.011) | 1.037 (0.009) | 0.04 (0.4) | 1.019 (0.008) | 31.0826/35.3518 |
| PZ5 | Fold | Aragonite | 9 | 18 (3) | 1.017 (0.005) | 1.035 (0.006) | -0.03 (0.38) | 1.017 (0.008) | 31.0826/35.3519 |
| PZ6 | Fold | Aragonite | 7 | 24 (9) | 1.006 (0.003) | 1.023 (0.003) | 0.44 (0.27) | 1.016 (0.003) | 31.0823/35.3527 |
| PZ7 | Fold | Aragonite | 9 | 19 (8.6) | 1.007 (0.003) | 1.037 (0.011) | 0.6 (0.17) | 1.029 (0.01) | 31.0823/35.3527 |
| PZ9 | Fold | Aragonite | 11 | 30 (7) | 1.019 (0.004) | 1.035 (0.007) | -0.13 (0.34) | 1.016 (0.008) | 31.0823/35.3529 |
| PZ9 | Fold | Detritus | 8 | 195 (22) | 1.012 (0.004) | 1.023 (0.003) | -0.047 (0.42) | 1.011 (0.006) | 31.0823/35.3529 |
| ALM1 | Fold upper anticline (horizontal layer) | Detritus | 6 | 81 (15) | 1.002* (0.005) | 1.034* (0.003) | 0.87* (0.27) | 1.032* (0.006) | 31.7975/35.4559 |
| ALM2 | Fold upper anticline (forelimb) | Detritus | 6 | 89 (11) | 1.01 (0.001) | 1.021 (0.001) | 0.07 (0.08) | 1.011 (0.001) | 31.7975/35.4559 |
| ALM1 | Fold hinge | Detritus | 7 | 63 (11) | 1.01 (0.003) | 1.024 (0.008) | 0.11 (0.36) | 1.014 (0.009) | 31.7975/35.4559 |
| MS1 | Breccia layer | Mostly aragonite | 22 | 49 (7.5) | 1.001* (m.) (0.001) | 1.016* (m.) (0.003) | 0.83* (m.) (0.11) | 1.014* (m.) (0.003) | 31.3072/35.3752 |
| MS2 | Breccia layer | Mostly aragonite | 5 | 24 (2.2) | 1.00(m.) (0.001) | 1.018(m.) (0.002) | 0.98(m.) (0.08) | 1.018(m.) (0.003) | 31.3073/35.3753 |
| MS3 (1-10) | Breccia layer | Mostly aragonite | 8 | 55 (6.8) | 1.002 (0.001) | 1.029 (0.002) | 0.84 (0.08) | 1.026 (0.001) | 31.3076/35.3755 |
| MS3 (11-28) | Breccia layer | Mostly aragonite | 17 | 38 (3) | 1.002* (m.) (0.003) | 1.027* (m.) (0.008) | 0.84* (m.) (0.13) | 1.025* (m.) (0.006) | 31.3076/35.3755 |
| MS4 | Breccia layer | Mostly aragonite | 10 | 43 (2) | 1.001* (m.) (0.001) | 1.026* (m.) (0.002) | 0.9* (m.) (0.06) | 1.025* (m.) (0.002) | 31.3074/35.3753 |
| MS5 | Injection clastic dike | Detritus | 8 | 47 (15) | 1.005 (0.003) | 1.013 (0.003) | 0.25 (0.28) | 1.008 (0.002) | 31.3076/35.3754 |

Table DR1. (continued)

| Site | Structure type | Rock type | *N* | $K_m$ | *L* [a] | *P* [a] | *T* [a] | *F* [a] | **Coordinates Lat./Lon.** |
|---|---|---|---|---|---|---|---|---|---|
| PZ8 | Injection clastic dike | Detritus | 11 | 39 (13) | 1.007 (0.004) | 1.017 (0.004) | 0.24 (0.35) | 1.01 (0.003) | 31.0984/35.3774 |
| TK | Injection clastic dike | Detritus | 17 | 64 (12) | 1.005(m.) (0.003) | 1.01(m.) (0.004) | 0.07(m.) (0.35) | 1.006(m.) (0.004) | 31.0942/35.3652 |
| TP | Injection clastic dike | Detritus | 26 | 66 (12) | 1.005 (0.002) | 1.009 (0.003) | -0.18 (0.34) | 1.004 (0.002) | 31.0831/35.3634 |
| TN | Injection clastic dike | Detritus | 24 | 114 (34) | 1.007 (0.003) | 1.015 (0.005) | 0.023 (0.4) | 1.008 (0.004) | 31.0861/35.3548 |
| QLOW | Injection clastic dike | Detritus | 7 | 96 (34) | 1.007 (0.001) | 1.016 (0.007) | -0.024 (0.37) | 1.008 (0.006) | 31.0905/35.3648 |
| Q | Injection clastic dike | Detritus | 5 | 63 (6) | 1.005 (0.003) | 1.009 (0.003) | -0.15 (0.57) | 1.004 (0.004) | 31.0905/35.3648 |
| TG (1-12) | Injection clastic dike | Detritus | 10 | 106 (46) | 1.009 (0.004) | 1.021 (0.005) | 0.048 (0.41) | 1.011 (0.005) | 31.0862/35.35518 |
| TG (L-U) | Injection clastic dike | Detritus | 6 | 90 (22) | 1.011 (0.004) | 1.019 (0.005) | -0.18 (0.4) | 1.008 (0.005) | 31.0862/35.35518 |
| TR-B | Injection clastic dike | Detritus | 13 | 199 (32) | 1.007 (0.002) | 1.011 (0.002) | -0.26 (0.45) | 1.004 (0.004) | 31.0862/35.35518 |
| TR-G | Injection clastic dike | Detritus | 10 | 132 (35) | 1.006 (0.002) | 1.011 (0.003) | -0.15 (0.3) | 1.005 (0.002) | 31.0862/35.35518 |
| TR-F | Injection clastic dike | Detritus | 11 | 93 (22) | 1.005 (0.002) | 1.012 (0.002) | 0.1 (0.25) | 1.006 (0.001) | 31.0862/35.35518 |
| Q (L-U) | Injection clastic dike | Detritus | 9 | 123 (20) | 1.005 (0.001) | 1.01 (0.003) | -0.1 (0.4) | 1.004 (0.003) | 31.0862/35.35518 |
| QC | Injection clastic dike | Detritus | 4 | 73 (6.5) | 1.004 (-) | 1.01 (-) | 0.27 (-) | 1.006 (-) | 31.0906/35.3647 |
| QD | Injection clastic dike | Detritus | 5 | 77 (8.1) | 1.003 (0.001) | 1.01 (0.002) | 0.49 (0.26) | 1.007 (0.001) | 31.0906/35.3648 |
| QE | Injection clastic dike | Detritus | 9 | 80 (6.9) | 1.004 (0.001) | 1.012 (0.002) | 0.4 (0.2) | 1.008 (0.002) | 31.0905/35.3648 |
| MS6 | Fault | Aragonite | 19 | 32 (10) | 1.008 (0.004) | 1.038 (0.004) | 0.6 (0.21) | 1.031 (0.005) | 31.3076/35.3756 |
| MM/Footwalll | Fault | Aragonite | 16 | 36 (16) | 1.008 (0.008) | 1.04 (0.011) | 0.63 (0.25) | 1.032 (0.006) | 31.3077/35.3757 |
| MM/Hangingwall | Fault | Aragonite | 9 | 36 (5) | 1.005 (0.003) | 1.043 (0.004) | 0.76 (0.14) | 1.038 (0.006) | 31.3077/35.3757 |
| MM/Intermediate block I | Fault | Aragonite | 13 | 27 (1.8) | 1.006 (0.003) | 1.039 (0.003) | 0.68 (0.18) | 1.032 (0.004) | 31.3077/35.3757 |
| MP/ Footwall | Fault | Aragonite | 12 | 38 (6.7) | 1.005 (0.003) | 1.039 (0.005) | 0.76 (0.1) | 1.035 (0.004) | 31.3077/35.3759 |
| MP/Hangingwall | Fault | Aragonite | 6 | 42 (8.3) | 1.004 (0.002) | 1.037 (0.004) | 0.76 (0.091) | 1.033 (0.004) | 31.3077/35.3759 |
| ZIN1 | Fault ( gouge) | Aragonite | 12 | 30 (6.5) | 1.012 (0.004) | 1.038 (0.006) | 0.38 (0.16) | 1.026 (0.004) | 30.9611/35.3021 |
| ZIN2 | Fault ( gouge) | Aragonite | 8 | 23 (9) | 1.014 (0.006) | 1.039 (0.009) | 0.3 (0.16) | 1.025 (0.005) | 30.9611/35.3021 |
| L-9 | Fault-sheared dike (gouge) | | 9 | 34 (16) | 1.008 (0.003) | 1.027 (0.006) | 0.44 (0.17) | 1.02 (0.005) | 31.0859/35.3577 |
| MM (41-52) | Sedimentary layer, near fault | Aragonite | 10 | 26 (3.7) | 1.001* (0.001) | 1.036* (0.003) | 0.91* (0.083) | 1.032* (0.003) | 31.3077/35.3757 |
| MM (13-22, 68 70-71) | Sedimentary layer, near fault | Aragonite | 13 | 29 (3.5) | 1.002* (0.003) | 1.031* (0.006) | 0.84* (0.18) | 1.029* (0.005) | 31.3077/35.3757 |
| MP (1-20) | Sedimentary layer, near fault | Aragonite | 24 | 47 (9.6) | 1.002* (0.005) | 1.034* (0.004) | 0.89* (0.28) | 1.032* (0.006) | 31.3077/35.3759 |
| MP (34-41) | Sedimentary layer, near fault | Aragonite | 7 | 37 (4.0) | 1.002* (0.001) | 1.035* (0.003) | 0.9* (0.064) | 1.033* (0.003) | 31.3077/35.3759 |

*Notes: N*, number of specimens; *k*m, mean susceptibility (in $10^{-6}$ SI units);
*L*, lineation; *P*, anisotropy degree; *T*, shape of the AMS ellipsoid. *mean tensor (Jelinek's statistics).
Standard deviation in parentheses.

Table DR2: Parts of fold built of aragonite

| Legend for *T-L* plot | Structural position | Symbol |
|---|---|---|
| MS10 | Upper anticline (horizontal layer) | A2 |
| MS10 | Forelimb | A1 |
| MS10 | Hinge | A3 |
| Zin2 | Upper anticline (horizontal layer) | B1 (ZN 1-6) |
| ZIN2 | Hinge | B2 (ZN 7-12) |
| ZIN2.1 | Hinge | B3 (ZN 13-20) |
| PZ3 | Upper anticline (slight tilted) | C1 |
| PZ3 | Lower limb (tilted layer) | C2 |
| PZ3 | Hinge | C3 |
| PZ5 | Upper anticline (horizontal layer) | D1 |
| PZ5 | Hinge | D2 |
| PZ5 | Upper anticline (horizontal layer) | D3 |
| PZ6 | Hangingwall anticline | E1 |
| PZ7 | Footwall anticline | E2 |
| PZ9 | Upper anticline (horizontal layer) | F1 |
| PZ9 | Hangingwall anticline (Forelimb) | F2 |
| ZIN1 | Hinge | G1 |
| ZIN1 | Footwall anticline | G2 |
| ZIN1 | Hangingwall anticline | G3 |

Table DR3: Parts of fold built of detritus

| Legend for *T-L* plot | Structural position | Symbol |
|---|---|---|
| ALM1 | Upper anticline (horizontal later) | A1 (AL 8-13) |
| ZIN2 | Upper anticline (horizontal later) | B1 (ZN2 21-28) |
| ALM2 | Hangingwall anticline (Forelimb) | C (AL 15-20) |
| ALM1 | Hinge | A2 (AL 1-7) |
| PZ9 | Hangingwall anticline (Forelimb) | D1 |
| PZ9 | Upper anticline (horizontal layer) | D2 |
| ZIN2 | Hinge | B2 (ZN 29-35) |

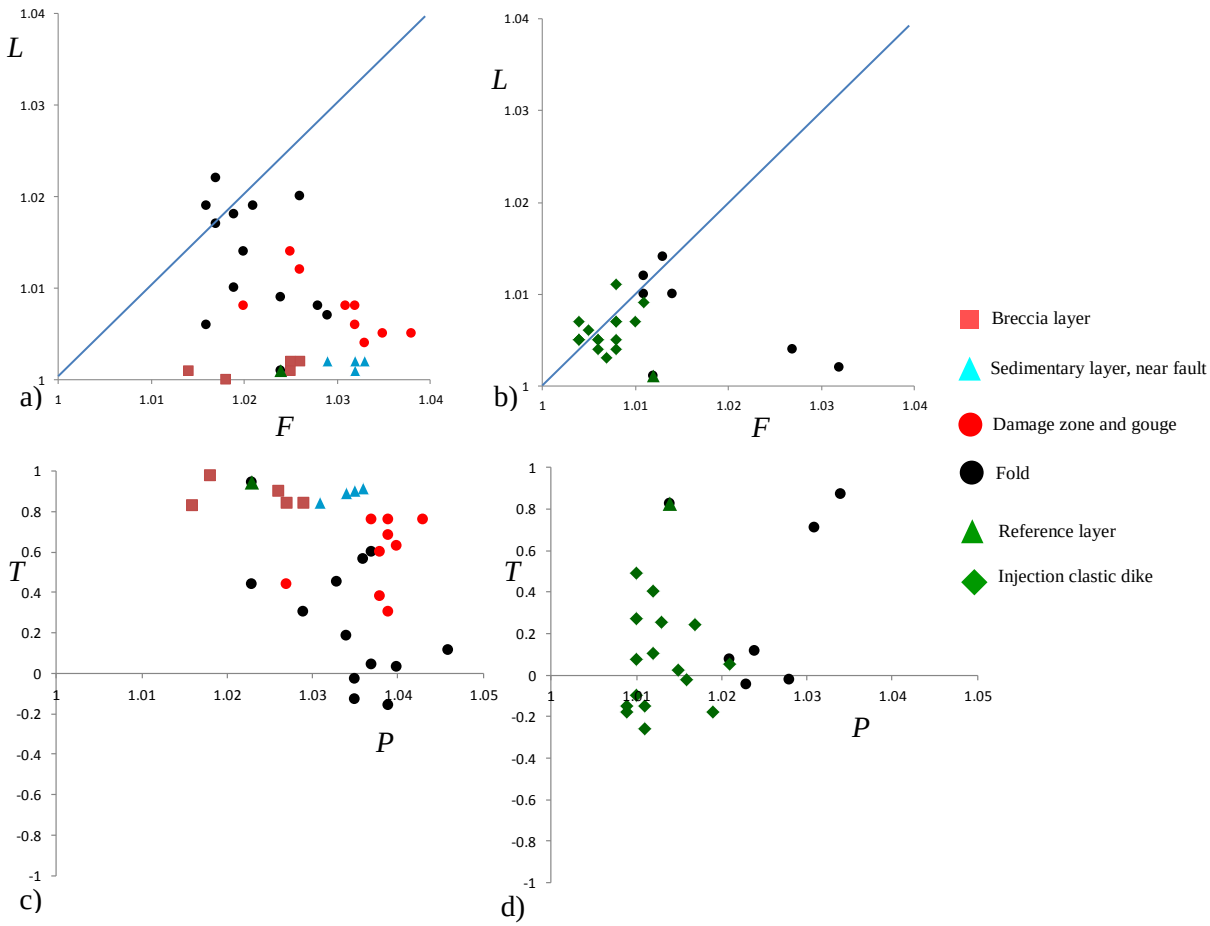


Figure DR1- Common biparametric plots of different seismite types containing aragonite and detritus layers. a) and b) show the *L-F* plots of the aragonite and detritus materials, respectively; c) and d) show the *T-P* plots of the aragonite and detritus layers, respectively.

DR1. (continued)

In order to relate magnetic fabrics of sedimentary rocks with different deformation processes, it is beneficial to look at data sets in different ways since all the bi-parametric plots quantify some aspect of the magnetic ellipsoid shape.

Flinn plot aims to examine how much a set of data is prolate or, alternatively, how much the data is more oblate. The distance from the origin of the plot (at $L=F=1$) can indicate the overall anisotropy. An examination of this plot in the case of the aragonite layers (DR4a) shows that the sites are scattered in the form of a cloud and are mostly displayed in the foliation zone without pointing to any process. Most data are characterized by an oblate ellipsoid. Because the distance from the origin of most sites is changeable, this criterion can help scarcely in the diagnosis of the seismite types and an indication of a clear progressive process.

In the case of detritus layers (DR4b), the sites of the folds and the injection dikes are dispersed almost equally between the "lineation zone" and the "foliation zone" and therefore this kind of criterion can hardly distinguish between the two seismite types. One might think that both groups share the same regression line. However, this interpretation may lead to the mistaken conclusion that both groups underwent the same progressive process, which is totally incorrect since the strain under folding conditions is not the same as under injection conditions.

The *T-P* plot shows the prolateness and the oblateness of the ellipsoids (below and above the x-axis), and the overall anisotropy is indicated by the x-axis. In the case of aragonite layers' (DR1c), the sites may be differentiated into two main groups: (1) breccia layer, sedimentary layer, near fault and the reference layer; and (2) Damage zone, gouge and folds. However, in group 2, the damage zone and folds' sites are very scattered (i.e., cloud shaped). This is verified by the lack of success in adapting any kind of regression line between the sites. This "lack of success" may also develop in the fold group built of detritus (DR1d), if we also include the sedimentary layer that is falling outside of the possible linear regression line.

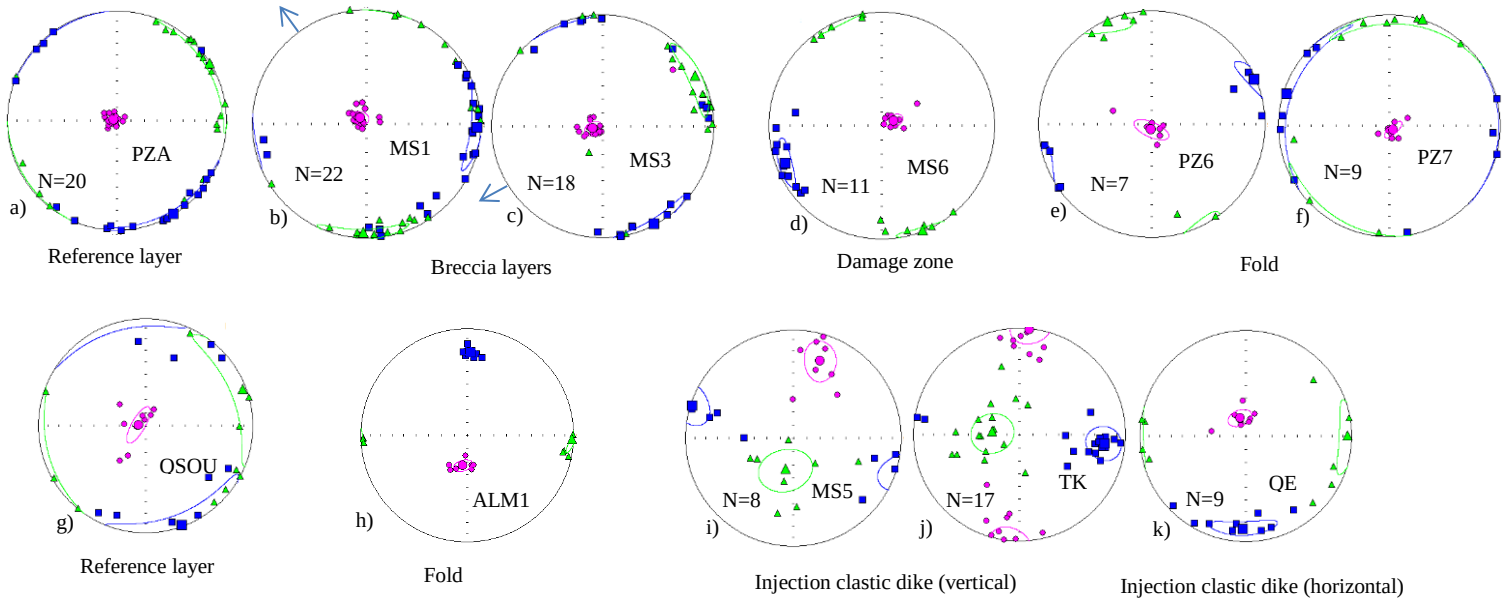


FigureDR2- Lower hemisphere, equal-area projection stereoplots of AMS principal axes, and the 95% confidence ellipses. The $K_1$, $K_2$, and $K_3$ axes are denoted by squares, triangle, and circles, respectively. Stereoplots (a)-(f) show the magnetic fabrics of the reference layer, breccia layers, damage zones and folds, respectively built of aragonite. Stereoplots (g)-(k) show the magnetic fabrics of the reference layer, folds and injection clastic dikes (vertical and horizontal flow), respectively, built of detritus layer.

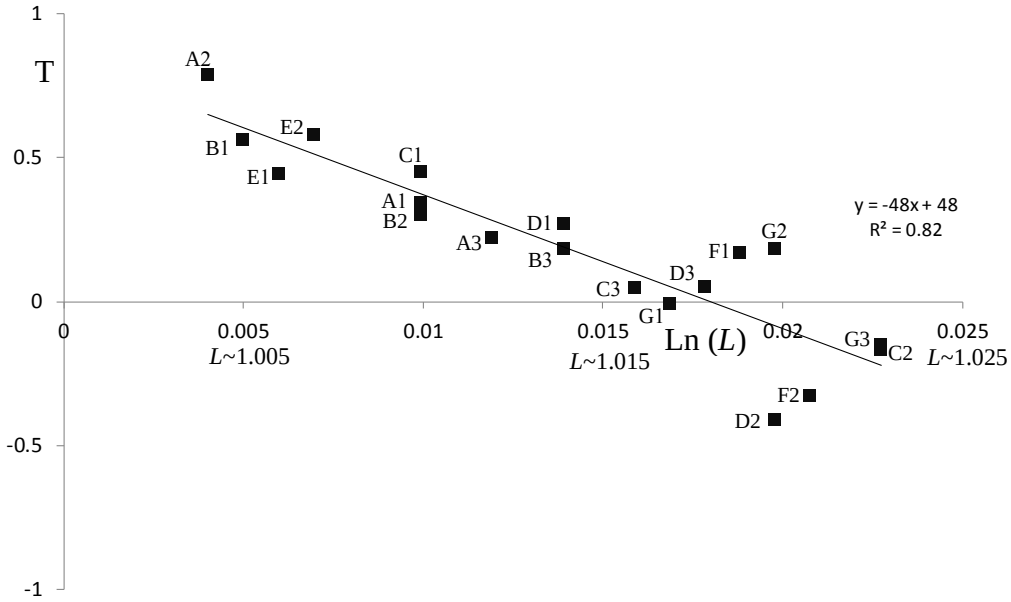


a)

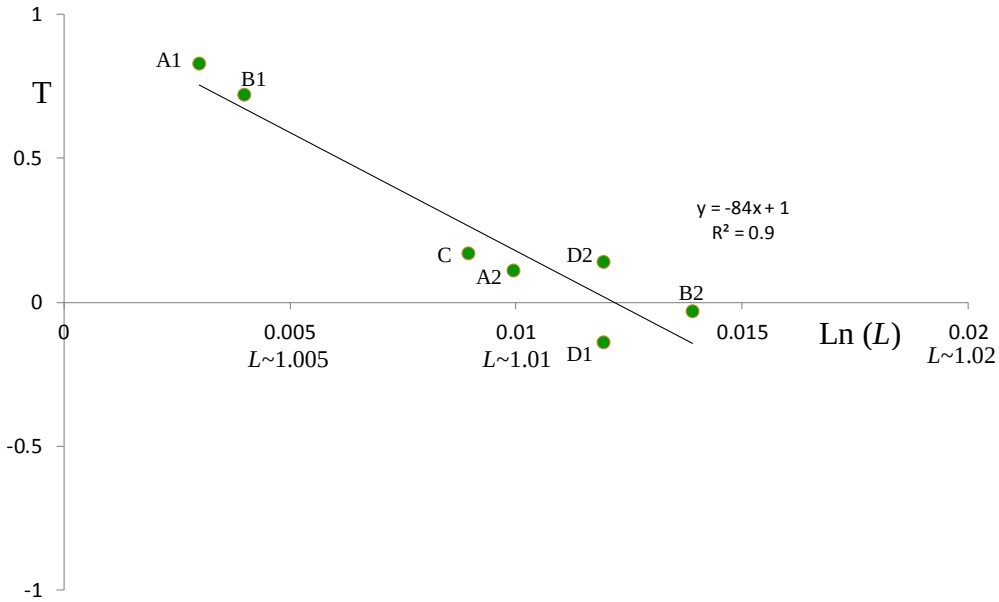


b)

Figure DR3- a) Different structural domains of folds (see Table 2) built of aragonite layers presented on *T-L* plot. b) Different structural domains of folds (see Table 3) built of detritus layers presented on *T-L* plot.